Analytical Expression for the Time-Domain Green's Function of a Discrete Plane Wave Propagating in a 3-D FDTD Grid

Tomasz P. Stefański, *Member, IEEE,* and Bartosz Reichel

***Abstract*—In this paper, a closed-form expression for the time-domain dyadic Green's function of a discrete plane wave (DPW) propagating in a 3-D finite-difference time-domain (FDTD) grid is derived. In order to verify our findings, the time-domain implementation of the DPW-injection technique is developed with the use of the derived expression for 3-D total-field/scattered-field (TFSF) FDTD simulations. This implementation requires computations of the time-domain Green's function of DPW with the use of multiple-precision arithmetic. Then, excitations at the TFSF interface can be computed as a time-domain convolution of a source function with the Green's function of DPW. The developed time-domain implementation of the DPW-injection technique demonstrates the leakage error across the TFSF interface around the numerical noise level that verifies the correctness of the derivation.**

***Index Terms*—Finite-difference time-domain (FDTD) methods.**

I. Introduction

PLANE-WAVE sources are required for calculations of the radar cross section (RCS) in the total-field/scattered-field (TFSF) formulation of the finite-difference time-domain (FDTD) method. Typical software implementations of TFSF FDTD involve a 1-D auxiliary incident field array that provides the plane wave excitation at the Huygens surface surrounding the scatterer (i.e., the TFSF interface). Due to the field leakage across the TFSF interface into the scattered-field region, this classical technique [1] has limited accuracy. Therefore, the topic of the plane wave injection in FDTD simulations has been investigated intensively for many years [2]–[7].

In [2]–[3], an analytic field propagator (AFP) technique is presented that solves numerically the FDTD dispersion relationship for the wavenumber $\mathbf{k}(\omega)$ and calculates the 1-D frequency-domain discrete Green's function (DGF) of the plane wave in the grid ($e^{-j\mathbf{k}(\omega)\cdot\mathbf{r}}$). Then, this DGF is employed for calculation of frequency-domain excitations at the TFSF interface. Finally, the time-domain excitations are computed for each point at the TFSF interface with the use of the inverse Fourier transform. The AFP technique has been later optimized by Tan *et al.* in order to reduce the consumption of memory [4]. This optimization takes the advantage of the inherent 1-D nature of plane waves and a consistent set of projection operators defined for rational angles of the plane wave propagation in the FDTD grid [5], [6]. Although this method allows one to obtain the leakage error at the machine precision level, still searching for roots of the FDTD dispersion relationship at the complex plane is required.

In [7], a technique is proposed for generation of discrete plane waves (DPWs) that are perfectly matched to the 3-D FDTD grid. This formulation is derived with the use of the 1-D properties of DPW and optimized projection of 3-D FDTD operators to the 1-D domain. This technique represents the state-of-the-art in the area of the plane wave injection in FDTD, because it is simultaneously efficient and accurate.

Despite development of techniques of perfect injection of DPW into the FDTD grid, time-domain DGF [8]–[11] has not yet been derived for DPW propagating in the 3-D FDTD grid to the best of our knowledge. It is well-known that the Green's function for a plane wave propagating in the $\mathbf{p}$-direction in the continuous domain is respectively represented by $e^{-j\tau\omega}$ and $\delta(t-\tau)$ in frequency and time domain ($\tau = \mathbf{p}\cdot\mathbf{r}/c$ denotes the retardation time, c denotes the speed of light, $\delta(t)$ denotes the Dirac's delta function). In the discrete domain, $e^{-j\mathbf{k}(\omega)\cdot\mathbf{r}}$ (where $\mathbf{k}(\omega)$ is obtained from the solution of the dispersion relationship) is frequency-domain DGF as demonstrated in [2], [3]. However, the formula for time-domain DGF of DPW in the 3-D FDTD grid has remained unknown. Therefore, we have investigated the plane wave propagation in the 3-D FDTD grid using methodology based on the multidimensional $\mathcal{Z}$–transform [12]. The closed-form expression for time-domain dyadic DGF of DPW in the 3-D grid is derived in this paper. Its purpose is to extend the earlier reported 2-D results [13] towards the 3-D grid. We present a comprehensive report on the derivation of DGF of DPW in the 3-D FDTD grid along with an evaluation of the leakage error across the TFSF interface. For the sake of this evaluation, the 3-D AFP technique is implemented in the time domain allowing us to compute excitations at the TFSF interface as a convolution of a source function with derived DGF. Results obtained demonstrate that the perfect injection of DPW can be achieved with the use of the derived DGF expression. Presented theoretical results facilitate investigations in the area of the discrete electromagnetic field theory and increase knowledge about TFSF FDTD simulations of scattering problems. This paper provides the development of the results shown in the earlier publications on the propagation of DPW in the FDTD grid [7], [13].

Manuscript received January 20, 2016. This work was supported by the Polish National Science Centre under Agreement DEC-2012/05/D/ST7/00141.

Tomasz P. Stefański is with the Faculty of Electronics, Telecommunications and Informatics, Gdansk University of Technology, Gdansk 80-233, Poland (e-mail:tomasz.stefanski@pg.gda.pl).

Bartosz Reichel is with the Faculty of Applied Physics and Mathematics, Gdansk University of Technology, Gdansk 80-233, Poland (e-mail:reichel@mif.pg.gda.pl).

II. Time-Domain Green's Function of DPW in 3-D FDTD grid

Let us consider 3-D FDTD update equations for electric (E) and magnetic (H) fields in an infinite free space

$$H_{x_{ij+\frac{1}{2}k+\frac{1}{2}}}^{n+\frac{1}{2}} = H_{x_{ij+\frac{1}{2}k+\frac{1}{2}}}^{n-\frac{1}{2}} + \frac{\Delta t}{\mu_0} \times \left(\frac{E_{y_{ij+\frac{1}{2}k+1}}^{n} - E_{y_{ij+\frac{1}{2}k}}^{n}}{\Delta z} - \frac{E_{z_{ij+1k+\frac{1}{2}}}^{n} - E_{z_{ijk+\frac{1}{2}}}^{n}}{\Delta y} \right) \tag{1a}$$

$$H_{y_{i+\frac{1}{2}jk+\frac{1}{2}}}^{n+\frac{1}{2}} = H_{y_{i+\frac{1}{2}jk+\frac{1}{2}}}^{n-\frac{1}{2}} + \frac{\Delta t}{\mu_0} \times \left(\frac{E_{z_{i+1jk+\frac{1}{2}}}^{n} - E_{z_{ijk+\frac{1}{2}}}^{n}}{\Delta x} - \frac{E_{x_{i+\frac{1}{2}jk+1}}^{n} - E_{x_{i+\frac{1}{2}jk}}^{n}}{\Delta z} \right) \tag{1b}$$

$$H_{z_{i+\frac{1}{2}j+\frac{1}{2}k}}^{n+\frac{1}{2}} = H_{z_{i+\frac{1}{2}j+\frac{1}{2}k}}^{n-\frac{1}{2}} + \frac{\Delta t}{\mu_0} \times \left(\frac{E_{x_{i+\frac{1}{2}j+1k}}^{n} - E_{x_{i+\frac{1}{2}jk}}^{n}}{\Delta y} - \frac{E_{y_{i+1j+\frac{1}{2}k}}^{n} - E_{y_{ij+\frac{1}{2}k}}^{n}}{\Delta x} \right) \tag{1c}$$

$$E_{x_{i+\frac{1}{2}jk}}^{n+1} = E_{x_{i+\frac{1}{2}jk}}^{n} + \frac{\Delta t}{\epsilon_0} \left(\frac{H_{z_{i+\frac{1}{2}j+\frac{1}{2}k}}^{n+\frac{1}{2}} - H_{z_{i+\frac{1}{2}j-\frac{1}{2}k}}^{n+\frac{1}{2}}}{\Delta y} - \frac{H_{y_{i+\frac{1}{2}jk+\frac{1}{2}}}^{n+\frac{1}{2}} - H_{y_{i+\frac{1}{2}jk-\frac{1}{2}}}^{n+\frac{1}{2}}}{\Delta z} - J_{x_{i+\frac{1}{2}jk}}^{n+\frac{1}{2}} \right) \tag{1d}$$

$$E_{y_{ij+\frac{1}{2}k}}^{n+1} = E_{y_{ij+\frac{1}{2}k}}^{n} + \frac{\Delta t}{\epsilon_0} \left(\frac{H_{x_{ij+\frac{1}{2}k+\frac{1}{2}}}^{n+\frac{1}{2}} - H_{x_{ij+\frac{1}{2}k-\frac{1}{2}}}^{n+\frac{1}{2}}}{\Delta z} - \frac{H_{z_{i+\frac{1}{2}j+\frac{1}{2}k}}^{n+\frac{1}{2}} - H_{z_{i-\frac{1}{2}j+\frac{1}{2}k}}^{n+\frac{1}{2}}}{\Delta x} - J_{y_{ij+\frac{1}{2}k}}^{n+\frac{1}{2}} \right) \tag{1e}$$

$$E_{z_{ijk+\frac{1}{2}}}^{n+1} = E_{z_{ijk+\frac{1}{2}}}^{n} + \frac{\Delta t}{\epsilon_0} \left(\frac{H_{y_{i+\frac{1}{2}jk+\frac{1}{2}}}^{n+\frac{1}{2}} - H_{y_{i-\frac{1}{2}jk+\frac{1}{2}}}^{n+\frac{1}{2}}}{\Delta x} - \frac{H_{x_{ij+\frac{1}{2}k+\frac{1}{2}}}^{n+\frac{1}{2}} - H_{x_{ij-\frac{1}{2}k+\frac{1}{2}}}^{n+\frac{1}{2}}}{\Delta y} - J_{z_{ijk+\frac{1}{2}}}^{n+\frac{1}{2}} \right). \tag{1f}$$

In (1a)–(1f), Δt is the time-step size, Δu is the discretization-step size along the u-direction ($u = x, y, z$), n is the time index, and i, j, k are the spatial indices in the grid. J denotes soft-source excitation of the grid. Let us consider DPW in the 3-D FDTD grid propagating in the direction specified by $\mathbf{p} = (p_x, p_y, p_z) = (\sin\theta\cos\phi, \sin\theta\sin\phi, \cos\theta)$ [7]. The planar wavefront equation is given by

$$r = p_x i\Delta x + p_y j\Delta y + p_z k\Delta z. \tag{2}$$

Denoting $\Delta r_u = p_u \Delta u$ (where $u = x, y, z$), (2) can be written as

$$r = i\Delta r_x + j\Delta r_y + k\Delta r_z. \tag{3}$$

Let us project (1a)–(1f) on this 1-D grid as presented in [7]

$$H_{x_{r+\frac{\Delta r_y}{2}+\frac{\Delta r_z}{2}}}^{n+\frac{1}{2}} = H_{x_{r+\frac{\Delta r_y}{2}+\frac{\Delta r_z}{2}}}^{n-\frac{1}{2}} + \frac{\Delta t}{\mu_0} \left(\frac{E_{y_{r+\frac{\Delta r_y}{2}+\Delta r_z}}^{n} - E_{y_{r+\frac{\Delta r_y}{2}}}^{n}}{\Delta z} - \frac{E_{z_{r+\Delta r_y+\frac{\Delta r_z}{2}}}^{n} - E_{z_{r+\frac{\Delta r_z}{2}}}^{n}}{\Delta y} \right) \tag{4a}$$

$$H_{y_{r+\frac{\Delta r_x}{2}+\frac{\Delta r_z}{2}}}^{n+\frac{1}{2}} = H_{y_{r+\frac{\Delta r_x}{2}+\frac{\Delta r_z}{2}}}^{n-\frac{1}{2}} + \frac{\Delta t}{\mu_0} \left(\frac{E_{z_{r+\Delta r_x+\frac{\Delta r_z}{2}}}^{n} - E_{z_{r+\frac{\Delta r_z}{2}}}^{n}}{\Delta x} - \frac{E_{x_{r+\frac{\Delta r_x}{2}+\Delta r_z}}^{n} - E_{x_{r+\frac{\Delta r_x}{2}}}^{n}}{\Delta z} \right) \tag{4b}$$

$$H_{z_{r+\frac{\Delta r_x}{2}+\frac{\Delta r_y}{2}}}^{n+\frac{1}{2}} = H_{z_{r+\frac{\Delta r_x}{2}+\frac{\Delta r_y}{2}}}^{n-\frac{1}{2}} + \frac{\Delta t}{\mu_0} \left(\frac{E_{x_{r+\frac{\Delta r_x}{2}+\Delta r_y}}^{n} - E_{x_{r+\frac{\Delta r_x}{2}}}^{n}}{\Delta y} - \frac{E_{y_{r+\Delta r_x+\frac{\Delta r_y}{2}}}^{n} - E_{y_{r+\frac{\Delta r_y}{2}}}^{n}}{\Delta x} \right) \tag{4c}$$

$$E_{x_{r+\frac{\Delta r_x}{2}}}^{n+1} = E_{x_{r+\frac{\Delta r_x}{2}}}^{n} + \frac{\Delta t}{\epsilon_0} \left(\frac{H_{z_{r+\frac{\Delta r_x}{2}+\frac{\Delta r_y}{2}}}^{n+\frac{1}{2}} - H_{z_{r+\frac{\Delta r_x}{2}-\frac{\Delta r_y}{2}}}^{n+\frac{1}{2}}}{\Delta y} - \frac{H_{y_{r+\frac{\Delta r_x}{2}+\frac{\Delta r_z}{2}}}^{n+\frac{1}{2}} - H_{y_{r+\frac{\Delta r_x}{2}-\frac{\Delta r_z}{2}}}^{n+\frac{1}{2}}}{\Delta z} - J_{x_{r+\frac{\Delta r_x}{2}}}^{n+\frac{1}{2}} \right) \tag{4d}$$

$$E_{y_{r+\frac{\Delta r_y}{2}}}^{n+1} = E_{y_{r+\frac{\Delta r_y}{2}}}^{n} + \frac{\Delta t}{\epsilon_0} \left(\frac{H_{x_{r+\frac{\Delta r_y}{2}+\frac{\Delta r_z}{2}}}^{n+\frac{1}{2}} - H_{x_{r+\frac{\Delta r_y}{2}-\frac{\Delta r_z}{2}}}^{n+\frac{1}{2}}}{\Delta z} - \frac{H_{z_{r+\frac{\Delta r_x}{2}+\frac{\Delta r_y}{2}}}^{n+\frac{1}{2}} - H_{z_{r-\frac{\Delta r_x}{2}+\frac{\Delta r_y}{2}}}^{n+\frac{1}{2}}}{\Delta x} - J_{y_{r+\frac{\Delta r_y}{2}}}^{n+\frac{1}{2}} \right) \tag{4e}$$

$$E_{z_{r+\frac{\Delta r_z}{2}}}^{n+1} = E_{z_{r+\frac{\Delta r_z}{2}}}^{n} + \frac{\Delta t}{\epsilon_0}\left(\frac{H_{y_{r+\frac{\Delta r_x}{2}+\frac{\Delta r_z}{2}}}^{n+\frac{1}{2}} - H_{y_{r-\frac{\Delta r_x}{2}+\frac{\Delta r_z}{2}}}^{n+\frac{1}{2}}}{\Delta x} - \frac{H_{x_{r+\frac{\Delta r_y}{2}+\frac{\Delta r_z}{2}}}^{n+\frac{1}{2}} - H_{x_{r-\frac{\Delta r_y}{2}+\frac{\Delta r_z}{2}}}^{n+\frac{1}{2}}}{\Delta y} - J_{z_{r+\frac{\Delta r_z}{2}}}^{n+\frac{1}{2}}\right). \quad (4f)$$

According to [6], DPW can propagate in directions from a countably infinite set of discretized angles. These angles are related by integer numbers m_x, m_y, m_z

$$\Delta r = \frac{\Delta r_x}{m_x} = \frac{\Delta r_y}{m_y} = \frac{\Delta r_z}{m_z} \quad (5)$$

where Δr denotes the spacing in the associated 1-D grid in r–domain ($r = i_r \Delta r$). The numbers m_x, m_y, m_z count the number of gridcells in the x, y, z directions, respectively [4]. Hence, from (3) one obtains

$$i_r = m_x i + m_y j + m_z k. \quad (6)$$

Finally, every cell (i, j, k) in the main grid is associated with the index i_r in the auxiliary 1-D grid. Hence, (4a)–(4f) can be written as

$$H_{x_{i_r+\frac{m_y}{2}+\frac{m_z}{2}}}^{n+\frac{1}{2}} = H_{x_{i_r+\frac{m_y}{2}+\frac{m_z}{2}}}^{n-\frac{1}{2}} \frac{\Delta t}{\mu_0}\left(\frac{E_{y_{i_r+\frac{m_y}{2}+m_z}}^{n} - E_{y_{i_r+\frac{m_y}{2}}}^{n}}{\Delta z} - \frac{E_{z_{i_r+m_y+\frac{m_z}{2}}}^{n} - E_{z_{i_r+\frac{m_z}{2}}}^{n}}{\Delta y}\right) \quad (7a)$$

$$H_{y_{i_r+\frac{m_x}{2}+\frac{m_z}{2}}}^{n+\frac{1}{2}} = H_{y_{i_r+\frac{m_x}{2}+\frac{m_z}{2}}}^{n-\frac{1}{2}} \frac{\Delta t}{\mu_0}\left(\frac{E_{z_{i_r+m_x+\frac{m_z}{2}}}^{n} - E_{z_{i_r+\frac{m_z}{2}}}^{n}}{\Delta x} - \frac{E_{x_{i_r+\frac{m_x}{2}+m_z}}^{n} - E_{x_{i_r+\frac{m_x}{2}}}^{n}}{\Delta z}\right) \quad (7b)$$

$$H_{z_{i_r+\frac{m_x}{2}+\frac{m_y}{2}}}^{n+\frac{1}{2}} = H_{z_{i_r+\frac{m_x}{2}+\frac{m_y}{2}}}^{n-\frac{1}{2}} \frac{\Delta t}{\mu_0}\left(\frac{E_{x_{i_r+\frac{m_x}{2}+m_y}}^{n} - E_{x_{i_r+\frac{m_x}{2}}}^{n}}{\Delta y} - \frac{E_{y_{i_r+m_x+\frac{m_y}{2}}}^{n} - E_{y_{i_r+\frac{m_y}{2}}}^{n}}{\Delta x}\right) \quad (7c)$$

$$E_{x_{i_r+\frac{m_x}{2}}}^{n+1} = E_{x_{i_r+\frac{m_x}{2}}}^{n} + \frac{\Delta t}{\epsilon_0}\left(\frac{H_{z_{i_r+\frac{m_x}{2}+\frac{m_y}{2}}}^{n+\frac{1}{2}} - H_{z_{i_r+\frac{m_x}{2}-\frac{m_y}{2}}}^{n+\frac{1}{2}}}{\Delta y} - \frac{H_{y_{i_r+\frac{m_x}{2}+\frac{m_z}{2}}}^{n+\frac{1}{2}} - H_{y_{i_r+\frac{m_x}{2}-\frac{m_z}{2}}}^{n+\frac{1}{2}}}{\Delta z} - J_{x_{i_r+\frac{m_x}{2}}}^{n+\frac{1}{2}}\right) \quad (7d)$$

$$E_{y_{i_r+\frac{m_y}{2}}}^{n+1} = E_{y_{i_r+\frac{m_y}{2}}}^{n} + \frac{\Delta t}{\epsilon_0}\left(\frac{H_{x_{i_r+\frac{m_y}{2}+\frac{m_z}{2}}}^{n+\frac{1}{2}} - H_{x_{i_r+\frac{m_y}{2}-\frac{m_z}{2}}}^{n+\frac{1}{2}}}{\Delta z} - \frac{H_{z_{i_r+\frac{m_x}{2}+\frac{m_y}{2}}}^{n+\frac{1}{2}} - H_{z_{i_r-\frac{m_x}{2}+\frac{m_y}{2}}}^{n+\frac{1}{2}}}{\Delta x} - J_{y_{i_r+\frac{m_y}{2}}}^{n+\frac{1}{2}}\right) \quad (7e)$$

$$E_{z_{i_r+\frac{m_z}{2}}}^{n+1} = E_{z_{i_r+\frac{m_z}{2}}}^{n} + \frac{\Delta t}{\epsilon_0}\left(\frac{H_{y_{i_r+\frac{m_x}{2}+\frac{m_z}{2}}}^{n+\frac{1}{2}} - H_{y_{i_r-\frac{m_x}{2}+\frac{m_z}{2}}}^{n+\frac{1}{2}}}{\Delta x} - \frac{H_{x_{i_r+\frac{m_y}{2}+\frac{m_z}{2}}}^{n+\frac{1}{2}} - H_{x_{i_r-\frac{m_y}{2}+\frac{m_z}{2}}}^{n+\frac{1}{2}}}{\Delta y} - J_{z_{i_r+\frac{m_z}{2}}}^{n+\frac{1}{2}}\right). \quad (7f)$$

Let us denote $\nabla_p^u f_q = \frac{f_{q+p} - f_{q-p}}{\Delta u}$. Then, (7a)–(7f) can be written as

$$H_{x_{i_{h,x}}}^{n+\frac{1}{2}} = H_{x_{i_{h,x}}}^{n-\frac{1}{2}} + \frac{\Delta t}{\mu_0}\left(\nabla_{\frac{m_z}{2}}^{z} E_{y_{i_{h,x}}}^{n} - \nabla_{\frac{m_y}{2}}^{y} E_{z_{i_{h,x}}}^{n}\right) \quad (8a)$$

where $i_{h,x} = i_r + \frac{m_y}{2} + \frac{m_z}{2}$,

$$H_{y_{i_{h,y}}}^{n+\frac{1}{2}} = H_{y_{i_{h,y}}}^{n-\frac{1}{2}} + \frac{\Delta t}{\mu_0}\left(\nabla_{\frac{m_x}{2}}^{x} E_{z_{i_{h,y}}}^{n} - \nabla_{\frac{m_z}{2}}^{z} E_{x_{i_{h,y}}}^{n}\right) \quad (8b)$$

where $i_{h,y} = i_r + \frac{m_x}{2} + \frac{m_z}{2}$,

$$H_{z_{i_{h,z}}}^{n+\frac{1}{2}} = H_{z_{i_{h,z}}}^{n-\frac{1}{2}} + \frac{\Delta t}{\mu_0}\left(\nabla_{\frac{m_y}{2}}^{y} E_{x_{i_{h,z}}}^{n} - \nabla_{\frac{m_x}{2}}^{x} E_{y_{i_{h,z}}}^{n}\right) \quad (8c)$$

where $i_{h,z} = i_r + \frac{m_x}{2} + \frac{m_y}{2}$,

$$E_{x_{i_{e,x}}}^{n+1} = E_{x_{i_{e,x}}}^{n} + \frac{\Delta t}{\epsilon_0}\left(\nabla_{\frac{m_y}{2}}^{y} H_{z_{i_{e,x}}}^{n+\frac{1}{2}} - \nabla_{\frac{m_z}{2}}^{z} H_{y_{i_{e,x}}}^{n+\frac{1}{2}} - J_{x_{i_{e,x}}}^{n+\frac{1}{2}}\right) \quad (8d)$$

where $i_{e,x} = i_r + \frac{m_x}{2}$,

$$E_{y_{i_{e,y}}}^{n+1} = E_{y_{i_{e,y}}}^{n} + \frac{\Delta t}{\epsilon_0}\left(\nabla_{\frac{m_z}{2}}^{z} H_{x_{i_{e,y}}}^{n+\frac{1}{2}} - \nabla_{\frac{m_x}{2}}^{x} H_{z_{i_{e,y}}}^{n+\frac{1}{2}} - J_{y_{i_{e,y}}}^{n+\frac{1}{2}}\right) \quad (8e)$$

where $i_{e,y} = i_r + \frac{m_y}{2}$,

$$E_{z_{i_{e,z}}}^{n+1} = E_{z_{i_{e,z}}}^{n} + \frac{\Delta t}{\epsilon_0}\left(\nabla_{\frac{m_x}{2}}^{x} H_{y_{i_{e,z}}}^{n+\frac{1}{2}} - \nabla_{\frac{m_y}{2}}^{y} H_{x_{i_{e,z}}}^{n+\frac{1}{2}} - J_{z_{i_{e,z}}}^{n+\frac{1}{2}}\right) \quad (8f)$$

where $i_{e,z} = i_r + \frac{m_z}{2}$.

Equations (8a)–(8f) are represented with the use of the 2-D $\mathcal{Z}$–transform [14]

$$F(\Omega, X) = \mathcal{Z}\{F_{i_r}^n\} = \sum_{n=-\infty}^{\infty} \sum_{i_r=-\infty}^{\infty} F_{i_r}^n \Omega^{-n} X^{-i_r}. \quad (9)$$

The inverse $\mathcal{Z}$–transform is given by

$$F_{i_r}^n = \mathcal{Z}^{-1}\{F(\Omega, X)\} = \frac{1}{(2\pi \mathrm{j})^2} \oint_{\gamma_\Omega} \oint_{\gamma_X} F(\Omega, X) \Omega^{n-1} X^{i_r - 1} \mathrm{d}\Omega \mathrm{d}X. \quad (10)$$

$$\left(\Omega^{\frac{1}{2}}-\Omega^{-\frac{1}{2}}\right)^2\mathbf{I}+\mathbf{A}^2=$$
$$\begin{bmatrix}\left(\Omega^{\frac{1}{2}}-\Omega^{-\frac{1}{2}}\right)^2-s_z^2D^2_{\frac{m_z}{2}}-s_y^2D^2_{\frac{m_y}{2}} & s_xD_{\frac{m_x}{2}}s_yD_{\frac{m_y}{2}} & s_xD_{\frac{m_x}{2}}s_zD_{\frac{m_z}{2}}\\ s_yD_{\frac{m_y}{2}}s_xD_{\frac{m_x}{2}} & \left(\Omega^{\frac{1}{2}}-\Omega^{-\frac{1}{2}}\right)^2-s_z^2D^2_{\frac{m_z}{2}}-s_x^2D^2_{\frac{m_x}{2}} & s_yD_{\frac{m_y}{2}}s_zD_{\frac{m_z}{2}}\\ s_zD_{\frac{m_z}{2}}s_xD_{\frac{m_x}{2}} & s_zD_{\frac{m_z}{2}}s_yD_{\frac{m_y}{2}} & \left(\Omega^{\frac{1}{2}}-\Omega^{-\frac{1}{2}}\right)^2-s_x^2D^2_{\frac{m_x}{2}}-s_y^2D^2_{\frac{m_y}{2}}\end{bmatrix} \tag{17}$$

Each integral is evaluated over a closed contour that must lie completely within the region of convergence of F and must encircle the origin counterclockwise in the plane of the respective variable [14]. If the above-mentioned conditions are fulfilled, (8a)–(8f) can be written in the $\mathcal{Z}$–transform domain as

$$(\Omega^{\frac{1}{2}}-\Omega^{-\frac{1}{2}})\mathbf{E}=\mathbf{A}\mathbf{H}-\frac{\Delta t}{\epsilon_0}\mathbf{J} \tag{11}$$

$$(\Omega^{\frac{1}{2}}-\Omega^{-\frac{1}{2}})\mathbf{H}=-\mathbf{A}\mathbf{E}. \tag{12}$$

In (11)–(12)

$$\mathbf{E}=\begin{bmatrix}E_x\\E_y\\E_z\end{bmatrix}\quad \mathbf{H}=\eta\begin{bmatrix}H_x\\H_y\\H_z\end{bmatrix}\quad \mathbf{J}=\begin{bmatrix}J_x\\J_y\\J_z\end{bmatrix} \tag{13}$$

$$\mathbf{A}=\begin{bmatrix}0 & -s_zD_{\frac{m_z}{2}} & s_yD_{\frac{m_y}{2}}\\ s_zD_{\frac{m_z}{2}} & 0 & -s_xD_{\frac{m_x}{2}}\\ -s_yD_{\frac{m_y}{2}} & s_xD_{\frac{m_x}{2}} & 0\end{bmatrix} \tag{14}$$

where $s_u=c\Delta t/\Delta u$ is the Courant number along the u-direction ($u=x,y,z$), c and η are respectively the speed of light and the intrinsic impedance in free space, and $D_pF=\mathcal{Z}\{F_p^n-F_{-p}^n\}=(X^p-X^{-p})F$. Substituting (11) into (12) and vice versa, the wave equations are obtained

$$\left[\left(\Omega^{\frac{1}{2}}-\Omega^{-\frac{1}{2}}\right)^2\mathbf{I}+\mathbf{A}^2\right]\mathbf{H}=\frac{\Delta t}{\epsilon_0}\mathbf{A}\mathbf{J} \tag{15}$$

$$\left[\left(\Omega^{\frac{1}{2}}-\Omega^{-\frac{1}{2}}\right)^2\mathbf{I}+\mathbf{A}^2\right]\mathbf{E}=-\frac{\Delta t}{\epsilon_0}\left(\Omega^{\frac{1}{2}}-\Omega^{-\frac{1}{2}}\right)\mathbf{J} \tag{16}$$

where $\mathbf{I}$ denotes the identity matrix and the wave operator $\left[\left(\Omega^{\frac{1}{2}}-\Omega^{-\frac{1}{2}}\right)^2\mathbf{I}+\mathbf{A}^2\right]$ is given by (17) (see top of the page). The Green's function of DPW is defined as the inverse of the wave operator in (15)–(16)

$$\mathbf{G}=\begin{bmatrix}G_{xx} & G_{xy} & G_{xz}\\ G_{yx} & G_{yy} & G_{yz}\\ G_{zx} & G_{zy} & G_{zz}\end{bmatrix}=\left[\left(\Omega^{\frac{1}{2}}-\Omega^{-\frac{1}{2}}\right)^2\mathbf{I}+\mathbf{A}^2\right]^{-1}. \tag{18}$$

Therefore, the solution of the wave equations (15)–(16) can be written in the $\mathcal{Z}$–transform domain as

$$\mathbf{H}=\frac{\Delta t}{\epsilon_0}\mathbf{G}\mathbf{A}\mathbf{J} \tag{19}$$

$$\mathbf{E}=-\frac{\Delta t}{\epsilon_0}\left(\Omega^{\frac{1}{2}}-\Omega^{-\frac{1}{2}}\right)\mathbf{G}\mathbf{J}. \tag{20}$$

The inverse of the wave-operator matrix (17) is calculated with the use of the symbolic mathematics software [15] under the assumption that the inverse matrix exists

$$\mathbf{G}=\begin{bmatrix}\omega^2-\zeta^2-\eta^2 & \xi\zeta & \xi\eta\\ \xi\zeta & \omega^2-\xi^2-\eta^2 & \zeta\eta\\ \xi\eta & \zeta\eta & \omega^2-\xi^2-\zeta^2\end{bmatrix}^{-1}$$
$$=\frac{1}{\omega^2\left(\xi^2+\zeta^2+\eta^2-\omega^2\right)}$$
$$\times\begin{bmatrix}\xi^2-\omega^2 & \xi\zeta & \xi\eta\\ \xi\zeta & \zeta^2-\omega^2 & \zeta\eta\\ \xi\eta & \zeta\eta & \eta^2-\omega^2\end{bmatrix} \tag{21}$$

where $\omega^2=\left(\Omega^{\frac{1}{2}}-\Omega^{-\frac{1}{2}}\right)^2$, $\xi=s_xD_{\frac{m_x}{2}}$, $\zeta=s_yD_{\frac{m_y}{2}}$, $\eta=s_zD_{\frac{m_z}{2}}$. For the sake of brevity, only the first row of $\mathbf{G}$ is derived below. Let us consider G_{xy} component

$$G_{xy}=\frac{\xi\zeta}{\omega^2\left(\xi^2+\zeta^2+\eta^2-\omega^2\right)}. \tag{22}$$

It can be expanded as

$$G_{xy}=-\frac{\xi\zeta}{\omega^4}\sum_{m=0}^{\infty}\left(\frac{\xi^2+\zeta^2+\eta^2}{\omega^2}\right)^m \tag{23}$$

for the region of convergence defined as

$$\left|\xi^2+\zeta^2+\eta^2\right|<\left|\omega^2\right|. \tag{24}$$

Then, expanding the power of the sum with the use of the multinomial theorem, one obtains

$$G_{xy}=-\sum_{m=0}^{\infty}\omega^{-2(m+2)}\times\sum_{\alpha+\beta+\gamma=m}\binom{m}{\alpha,\beta,\gamma}\xi^{2\alpha}\zeta^{2\beta+1}\eta^{2\gamma}. \tag{25}$$

Hence, this component of the Green's function can be calculated in the time domain based on (10) as

$$G_{xy}{}_{i_r}^{n}=-\frac{1}{(2\pi\mathrm{j})^2}\sum_{m=0}^{\infty}\oint_{\gamma_\Omega}\frac{\Omega^{n-1}\mathrm{d}\Omega}{(\Omega-2+\Omega^{-1})^{m+2}}$$
$$\times\sum_{\alpha+\beta+\gamma=m}\binom{m}{\alpha,\beta,\gamma}s_x^{2\alpha+1}s_y^{2\beta+1}s_z^{2\gamma}$$
$$\times\oint_{\gamma_X}\left(X^{\frac{m_x}{2}}-X^{-\frac{m_x}{2}}\right)^{2\alpha+1}\left(X^{\frac{m_y}{2}}-X^{-\frac{m_y}{2}}\right)^{2\beta+1}$$
$$\times\left(X^{\frac{m_z}{2}}-X^{-\frac{m_z}{2}}\right)^{2\gamma}X^{i_r-1}\mathrm{d}X. \tag{26}$$

The integral in Ω-domain is calculated with the use of the Cauchy integral formula for derivatives

$$\frac{1}{2\pi \mathrm{j}} \oint_{\gamma_\Omega} \frac{\Omega^{n-1} \mathrm{d}\Omega}{(\Omega - 2 + \Omega^{-1})^{m+2}} = \begin{cases} \binom{m+n+1}{2m+3}, & n \geq m+2 \\ 0, & \text{otherwise} \end{cases}. \tag{27}$$

The contour γ_Ω is in the region of convergence of (10) which encloses $\Omega = 0$ and $\Omega = 1$. The integral in X-domain can be calculated with the use of the binomial theorem and the Cauchy integral formula as follows:

$$\begin{aligned} &\frac{1}{2\pi \mathrm{j}} \oint_{\gamma_X} \left(X^{\frac{m_x}{2}} - X^{-\frac{m_x}{2}}\right)^{2\alpha+1} \left(X^{\frac{m_y}{2}} - X^{-\frac{m_y}{2}}\right)^{2\beta+1} \\ &\times \left(X^{\frac{m_z}{2}} - X^{-\frac{m_z}{2}}\right)^{2\gamma} X^{i_r - 1} \mathrm{d}X \\ &= \sum_{p=0}^{2\alpha+1} \sum_{q=0}^{2\beta+1} \sum_{r=0}^{2\gamma} (-1)^{p+q+r} \binom{2\alpha+1}{p} \binom{2\beta+1}{q} \binom{2\gamma}{r} \\ &\times \frac{1}{2\pi \mathrm{j}} \oint_{\gamma_X} X^{m_x(\alpha - p + \frac{1}{2}) + m_y(\beta - q + \frac{1}{2}) + m_z(\gamma - r) + i_r - 1} \mathrm{d}X \\ &= \sum_{p=0}^{2\alpha+1} \sum_{q=0}^{2\beta+1} \sum_{r=0}^{2\gamma} (-1)^{p+q+r} \binom{2\alpha+1}{p} \binom{2\beta+1}{q} \binom{2\gamma}{r} \\ &\times \delta_{i_r, m_x(p-\alpha-\frac{1}{2}) + m_y(q-\beta-\frac{1}{2}) + m_z(r-\gamma)} \\ &= \sum_{\substack{p=0}}^{2\alpha+1} \sum_{q=0}^{2\beta+1} \sum_{r=0}^{2\gamma} (-1)^{p+q+r} \\ &\quad {\scriptstyle i_r = m_x(p-\alpha-\frac{1}{2}) + m_y(q-\beta-\frac{1}{2}) + m_z(r-\gamma)} \\ &\times \binom{2\alpha+1}{p} \binom{2\beta+1}{q} \binom{2\gamma}{r}. \end{aligned} \tag{28}$$

The contour γ_X is such that condition (24) is satisfied. In (28), $\delta_{a,b}$ denotes the Kronecker delta function. Hence, one obtains

$$\begin{aligned} G_{xy}{}^{\,n}_{i_r} &= \sum_{m=0}^{n-2} \binom{m+n+1}{2m+3} \\ &\times \sum_{\alpha+\beta+\gamma=m} \binom{m}{\alpha,\beta,\gamma} s_x^{2\alpha+1} s_y^{2\beta+1} s_z^{2\gamma} \\ &\times \sum_{\substack{p=0}}^{2\alpha+1} \sum_{q=0}^{2\beta+1} \sum_{r=0}^{2\gamma} (-1)^{p+q+r+1} \\ &\quad {\scriptstyle i_r = m_x(p-\alpha-\frac{1}{2}) + m_y(q-\beta-\frac{1}{2}) + m_z(r-\gamma)} \\ &\times \binom{2\alpha+1}{p} \binom{2\beta+1}{q} \binom{2\gamma}{r}. \end{aligned} \tag{29}$$

Analogously, it can be derived that

$$\begin{aligned} G_{xz}{}^{\,n}_{i_r} &= \sum_{m=0}^{n-2} \binom{m+n+1}{2m+3} \\ &\times \sum_{\alpha+\beta+\gamma=m} \binom{m}{\alpha,\beta,\gamma} s_x^{2\alpha+1} s_y^{2\beta} s_z^{2\gamma+1} \\ &\times \sum_{\substack{p=0}}^{2\alpha+1} \sum_{q=0}^{2\beta} \sum_{r=0}^{2\gamma+1} (-1)^{p+q+r+1} \\ &\quad {\scriptstyle i_r = m_x(p-\alpha-\frac{1}{2}) + m_y(q-\beta) + m_z(r-\gamma-\frac{1}{2})} \\ &\times \binom{2\alpha+1}{p} \binom{2\beta}{q} \binom{2\gamma+1}{r}. \end{aligned} \tag{30}$$

Then, let us consider G_{zz} component in the $\mathcal{Z}$–transform domain

$$G_{zz} = F_{zz} - K_{zz} \tag{31}$$

where

$$F_{zz} = \frac{\xi^2}{\omega^2 \left(\xi^2 + \zeta^2 + \eta^2 - \omega^2\right)} \tag{32}$$

$$K_{zz} = \frac{1}{\xi^2 + \zeta^2 + \eta^2 - \omega^2}. \tag{33}$$

We thus obtain in the time domain

$$G_{zz}{}^{\,n}_{i_r} = F_{zz}{}^{\,n}_{i_r} - K_{zz}{}^{\,n}_{i_r}. \tag{34}$$

$F_{zz}{}^{\,n}_{i_r}$ component is derived analogously as $G_{xy}{}^{\,n}_{i_r}$ component above

$$\begin{aligned} F_{zz}{}^{\,n}_{i_r} &= \sum_{m=0}^{n-2} \binom{m+n+1}{2m+3} \\ &\times \sum_{\alpha+\beta+\gamma=m} \binom{m}{\alpha,\beta,\gamma} s_x^{2\alpha+2} s_y^{2\beta} s_z^{2\gamma} \\ &\times \sum_{\substack{p=0}}^{2\alpha+2} \sum_{q=0}^{2\beta} \sum_{r=0}^{2\gamma} (-1)^{p+q+r+1} \\ &\quad {\scriptstyle i_r = m_x(p-\alpha-1) + m_y(q-\beta) + m_z(r-\gamma)} \\ &\times \binom{2\alpha+2}{p} \binom{2\beta}{q} \binom{2\gamma}{r}. \end{aligned} \tag{35}$$

$K_{zz}{}^{\,n}_{i_r}$ component can be expanded as

$$K_{zz} = -\frac{1}{\omega^2} \sum_{m=0}^{\infty} \left(\frac{\xi^2 + \zeta^2 + \eta^2}{\omega^2}\right)^m \tag{36}$$

for the region of convergence defined in (24). Expanding the power of the sum with the use of the multinomial theorem in the next step, one obtains

$$\begin{aligned} K_{zz} &= -\sum_{m=0}^{\infty} \omega^{-2(m+1)} \\ &\times \sum_{\alpha+\beta+\gamma=m} \binom{m}{\alpha,\beta,\gamma} \xi^{2\alpha} \zeta^{2\beta} \eta^{2\gamma}. \end{aligned} \tag{37}$$

Hence, one obtains in the time domain

$$K_{zz}{}^{\,n}_{i_r} = -\frac{1}{(2\pi\mathrm{j})^2}\sum_{m=0}^{\infty}\oint_{\gamma_\Omega}\frac{\Omega^{n-1}\mathrm{d}\Omega}{(\Omega-2+\Omega^{-1})^{m+1}} \times\sum_{\alpha+\beta+\gamma=m}\binom{m}{\alpha,\beta,\gamma}s_x^{2\alpha}s_y^{2\beta}s_z^{2\gamma} \times\oint_{\gamma_X}\left(X^{\frac{m_x}{2}}-X^{-\frac{m_x}{2}}\right)^{2\alpha}\left(X^{\frac{m_y}{2}}-X^{-\frac{m_y}{2}}\right)^{2\beta} \times\left(X^{\frac{m_z}{2}}-X^{-\frac{m_z}{2}}\right)^{2\gamma}X^{i_r-1}\mathrm{d}X. \quad (38)$$

Again, the integral in Ω-domain is calculated with the use of the Cauchy integral formula for derivatives

$$\frac{1}{2\pi\mathrm{j}}\oint_{\gamma_\Omega}\frac{\Omega^{n-1}\mathrm{d}\Omega}{(\Omega-2+\Omega^{-1})^{m+1}} = \begin{cases}\binom{m+n}{2m+1}, & n\geq m+1\\ 0, & \text{otherwise}\end{cases} \quad (39)$$

where the contour γ_Ω is in the region of convergence of (10) which encloses $\Omega=0$ and $\Omega=1$. The integral in X-domain can be calculated as presented above. Hence, one obtains

$$K_{zz}{}^{\,n}_{i_r} = \sum_{m=0}^{n-1}\binom{m+n}{2m+1} \times\sum_{\alpha+\beta+\gamma=m}\binom{m}{\alpha,\beta,\gamma}s_x^{2\alpha}s_y^{2\beta}s_z^{2\gamma} \times\sum_{p=0}^{2\alpha}\sum_{q=0}^{2\beta}\sum_{r=0}^{2\gamma}(-1)^{p+q+r+1} \quad i_r=m_x(p-\alpha)+m_y(q-\beta)+m_z(r-\gamma) \times\binom{2\alpha}{p}\binom{2\beta}{q}\binom{2\gamma}{r}. \quad (40)$$

The other components of dyadic DGF of DPW can be obtained by a suitable rotation of the subscripts x,y,z and the corresponding summation indices α,β,γ.

Finally, the electromagnetic field of DPW can be calculated in the time domain as

$$\mathbf{H}_{i_r}^{n+\frac{1}{2}} = \frac{\Delta t}{\epsilon_0}\sum_{n'=0}^{n}\sum_{i'_r}\mathbf{G}_{i_r-i'_r}^{n-n'} \times(c\Delta t)\begin{bmatrix}0 & -\nabla^z_{\frac{m_z}{2}} & \nabla^y_{\frac{m_y}{2}}\\ \nabla^z_{\frac{m_z}{2}} & 0 & -\nabla^x_{\frac{m_x}{2}}\\ -\nabla^y_{\frac{m_y}{2}} & \nabla^x_{\frac{m_x}{2}} & 0\end{bmatrix}\mathbf{J}_{i'_r}^{n'+\frac{1}{2}} \quad (41)$$

$$\mathbf{E}_{i_r}^{n} = -\frac{\Delta t}{\epsilon_0}\sum_{n'=0}^{n-1}\sum_{i'_r}\mathbf{G}_{i_r-i'_r}^{n-n'}\left(\mathbf{J}_{i'_r}^{n'+\frac{1}{2}}-\mathbf{J}_{i'_r}^{n'-\frac{1}{2}}\right) \quad (42)$$

where

$$\mathbf{E}\,{}^{\,n}_{i_r} = \begin{bmatrix}E_x\,{}^{\,n}_{i_r}\\ E_y\,{}^{\,n}_{i_r}\\ E_z\,{}^{\,n}_{i_r}\end{bmatrix}\quad \mathbf{H}\,{}^{\,n}_{i_r} = \eta\begin{bmatrix}H_x\,{}^{\,n}_{i_r}\\ H_y\,{}^{\,n}_{i_r}\\ H_z\,{}^{\,n}_{i_r}\end{bmatrix}\quad \mathbf{J}\,{}^{\,n}_{i_r} = \begin{bmatrix}J_x\,{}^{\,n}_{i_r}\\ J_y\,{}^{\,n}_{i_r}\\ J_z\,{}^{\,n}_{i_r}\end{bmatrix}. \quad (43)$$

The components of the Green's function

$$\mathbf{G}\,{}^{\,n}_{i_r} = \begin{bmatrix}G_{xx}\,{}^{\,n}_{i_r} & G_{xy}\,{}^{\,n}_{i_r} & G_{xz}\,{}^{\,n}_{i_r}\\ G_{yx}\,{}^{\,n}_{i_r} & G_{yy}\,{}^{\,n}_{i_r} & G_{yz}\,{}^{\,n}_{i_r}\\ G_{zx}\,{}^{\,n}_{i_r} & G_{zy}\,{}^{\,n}_{i_r} & G_{zz}\,{}^{\,n}_{i_r}\end{bmatrix} \quad (44)$$

are derived as presented above. In (41)–(42), the operators are applied to the excitation $\mathbf{J}$ instead of the kernel $\mathbf{G}$. Since the DGF equations are cumbersome for computations, the computational overhead can be reduced in this way. Formally, (41)–(42) can still be written in the standard form as follows:

$$\mathbf{H}_{i_r}^{n+\frac{1}{2}} = \frac{\Delta t}{\epsilon_0}\sum_{n'=0}^{n}\sum_{i'_r}\mathbf{G}_{\mathbf{hj}\,i_r-i'_r}^{n-n'}(c\Delta t\mathbf{J}_{i'_r}^{n'+\frac{1}{2}}) \quad (45)$$

$$\mathbf{E}_{i_r}^{n} = -\frac{\Delta t}{\epsilon_0}\sum_{n'=0}^{n-1}\sum_{i'_r}\mathbf{G}_{\mathbf{ej}\,i_r-i'_r}^{n-n'}\mathbf{J}_{i'_r}^{n'+\frac{1}{2}} \quad (46)$$

where

$$\mathbf{G}_{\mathbf{hj}}\,{}^{\,n}_{i_r} = \begin{bmatrix}\nabla^z_{\frac{m_z}{2}}G_{xy}\,{}^{\,n}_{i_r} & \nabla^x_{\frac{m_x}{2}}G_{xz}\,{}^{\,n}_{i_r} & \nabla^y_{\frac{m_y}{2}}G_{xx}\,{}^{\,n}_{i_r}\\ \nabla^z_{\frac{m_z}{2}}G_{yy}\,{}^{\,n}_{i_r} & \nabla^x_{\frac{m_x}{2}}G_{yz}\,{}^{\,n}_{i_r} & \nabla^y_{\frac{m_y}{2}}G_{yx}\,{}^{\,n}_{i_r}\\ \nabla^z_{\frac{m_z}{2}}G_{zy}\,{}^{\,n}_{i_r} & \nabla^x_{\frac{m_x}{2}}G_{zz}\,{}^{\,n}_{i_r} & \nabla^y_{\frac{m_y}{2}}G_{zx}\,{}^{\,n}_{i_r}\end{bmatrix} - \begin{bmatrix}\nabla^y_{\frac{m_y}{2}}G_{xz}\,{}^{\,n}_{i_r} & \nabla^z_{\frac{m_z}{2}}G_{xx}\,{}^{\,n}_{i_r} & \nabla^x_{\frac{m_x}{2}}G_{xy}\,{}^{\,n}_{i_r}\\ \nabla^y_{\frac{m_y}{2}}G_{yz}\,{}^{\,n}_{i_r} & \nabla^z_{\frac{m_z}{2}}G_{yx}\,{}^{\,n}_{i_r} & \nabla^x_{\frac{m_x}{2}}G_{yy}\,{}^{\,n}_{i_r}\\ \nabla^y_{\frac{m_y}{2}}G_{zz}\,{}^{\,n}_{i_r} & \nabla^z_{\frac{m_z}{2}}G_{zx}\,{}^{\,n}_{i_r} & \nabla^x_{\frac{m_x}{2}}G_{zy}\,{}^{\,n}_{i_r}\end{bmatrix} \quad (47)$$

$$\mathbf{G}_{\mathbf{ej}}\,{}^{\,n}_{i_r} = \mathbf{G}\,{}^{\,n}_{i_r} - \mathbf{G}\,{}^{\,n-1}_{i_r}. \quad (48)$$

However, in the presented numerical results, (41)–(42) are employed in order to save computational runtime. As seen, the components of dyadic DGF for DPW (29), (30), (35), (40) are similar to expressions for FDTD-compatible DGF [12]. Although both DGFs are based on combinatorial expressions, DGF of DPW contains decision functions which filter out inadmissible combinatorics in those expressions.

III. Numerical Results

The method is implemented in C programming language and tested on a machine with Intel i7-3770 3.4 GHz processor and Nvidia Gtx 660 graphics processing unit. Derived DGF of DPW involves binomial coefficients whose values may be large integers for high upper indices, whereas powers of the Courant numbers may be very small real numbers. Therefore, numerical difficulties can be expected if derived DGF is implemented in a common programming language with fixed-precision arithmetic. The implementation of DGF in software requires the application of multiple-precision arithmetic (MPA) [16], whose digits of precision are only limited by the size of the available memory in a computing system. In our work, multiple precision integers and rationals (MPIR) [17] and CUDA multiple precision arithmetic (CUMP) [18] libraries are employed. Although DGF computations require MPA, final results of the DGF generation are cast to double precision. However, other computations (e.g., the convolutions (41)–(42)) are implemented in double precision.

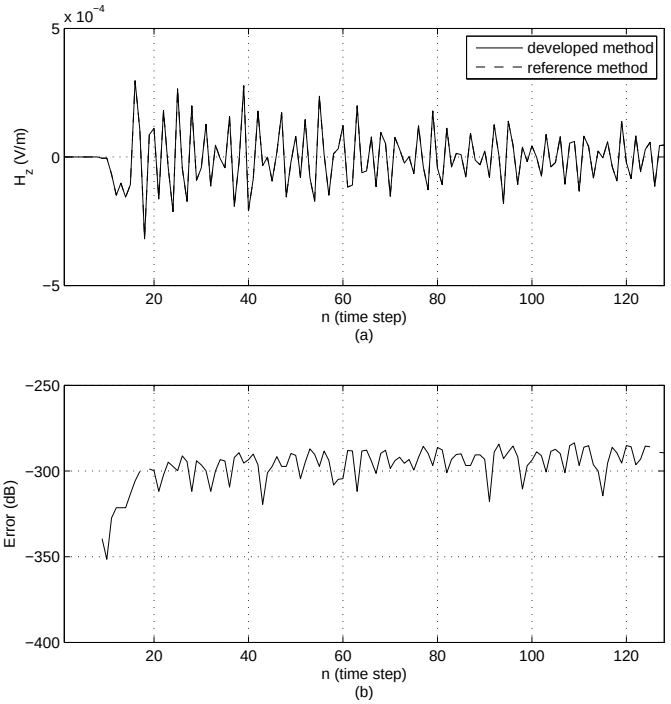

Fig. 1. (a) H_z component of the plane wave field computed with the use of the developed method and the reference method. Both waveforms overlap. (b) Relative error between both methods. Discontinuity of the line means that both methods computed exactly the same result in double precision.

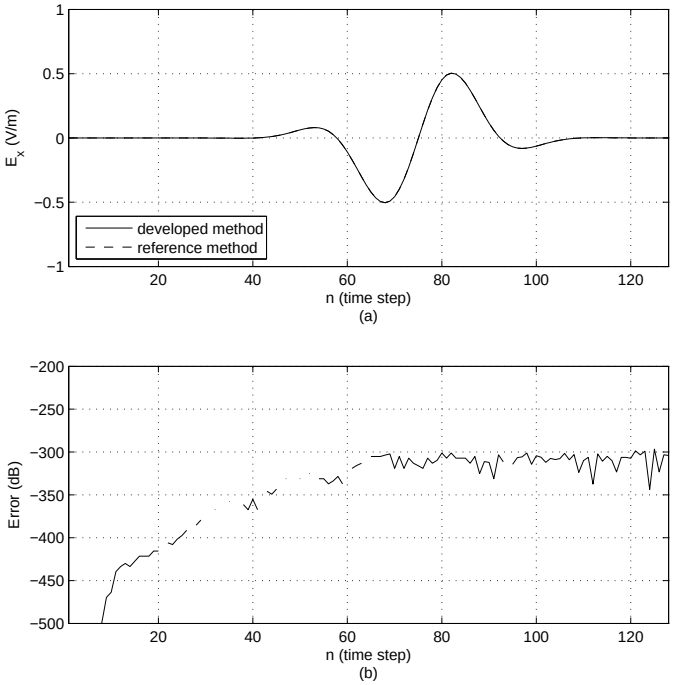

Fig. 2. (a) Convolution of the Gaussian-modulated harmonic signal with DGF (developed method) against waveform obtained with the use of the direct update of the FDTD-DPW grid (reference method). Both waveforms overlap. (b) Relative error between both methods. Discontinuity of the line means that both methods computed exactly the same result in double precision.

The spatial-step size is taken as $\Delta x = \Delta y = \Delta z = 1$ mm and the Courant numbers are taken as $s_x = s_y = s_z = 1/\sqrt{3}$ for the results presented here. Numerical tests are executed to validate the correctness of the DGF derivation. The relative error between waveforms generated with the use of the derived expression (f^n) and the reference method (f^n_{ref}) is defined as follows:

$$\text{Error} = 20 \log_{10} \frac{\left| f^n - f^n_{ref} \right|}{\max \left| f^n_{ref} \right|} \quad \text{(dB)}. \tag{49}$$

In the first test, H_z component of the plane wave field is computed for the excitation with the use of the Kronecker delta ($-\frac{\Delta t}{\epsilon_0} J^{n+\frac{1}{2}}_{i_r} = \delta_{i_r,i_s}\delta_{n,0}\hat{i}_x$). Fig. 1a presents the comparison between results computed with the use of the developed method (41)–(42) and those obtained from the FDTD-DPW method [7] formulated by (7a)–(7f) (reference method). The direction of the wave propagation is set to $\phi = 78.7°$, $\theta = 68.6°$ and $\psi = 11.3°$ ($m_x = 1$, $m_y = 5$, $m_z = 2$). The observation point is placed 32 cells away from the source. Fig. 1b presents the error between both methods. The error is around the numerical noise level. It validates the correctness of the DGF derivation.

Fig. 2a presents the comparison between the convolution (42) of the Gaussian-modulated harmonic signal (frequency range 5–25 GHz) with DGF, and the reference result obtained from the direct update of the FDTD-DPW grid. The direction of the wave propagation is set to $\phi = 68.2°$, $\theta = 60.9°$ and $\psi = 21.8°$ ($m_x = 2$, $m_y = 5$, $m_z = 3$). The observation point is also placed 32 cells away from the source in the FDTD-DPW grid. Fig. 2b presents the error between both methods. The correctness of the convolution computations is validated by the error around the numerical noise level.

Finally, the AFP technique is implemented in the time domain for the plane wave injection in 3-D TFSF FDTD simulations. The incident field at the TFSF interface is computed with the use of the time-domain formulation (41)–(42). The developed code is optimized taking advantage of the inherent 1-D nature of the plane wave as in the optimized AFP implementation [4]. In the test of the developed time-domain AFP technique, the total-field region is of size $21 \times 21 \times 21$ cells, whereas the FDTD domain is of size $680 \times 680 \times 680$ cells. The direction of the wave propagation is set to $\phi = 63.4°$, $\theta = 36.7°$ and $\psi = 26.6°$ ($m_x = 1$, $m_y = 2$, $m_z = 3$). The harmonic signal of frequency 30 GHz is employed as a soft source. Usually, several boundary points ($m = \max(|m_x|, |m_y|, |m_z|)$) are hard-sourced in order to initiate the wave propagating along a source grid [5], [7]. In the reported investigations, m points are soft-sourced by the same signal, which does not affect the match between the main grid and results of the DGF-based computations (41)–(42). However, the application of a soft source for the plane wave injection in the developed method makes the shape of the propagating wave different to the one obtained from hard sourcing of the FDTD-DPW grid (as implemented in [7]).

In Fig. 3, E_z field in the total-field region of the domain without a scatterer is presented for $n = 130$ time steps. The computational domain is cut in the centre plane $k = 340$. There are no visible reflections in the scattered-field region,

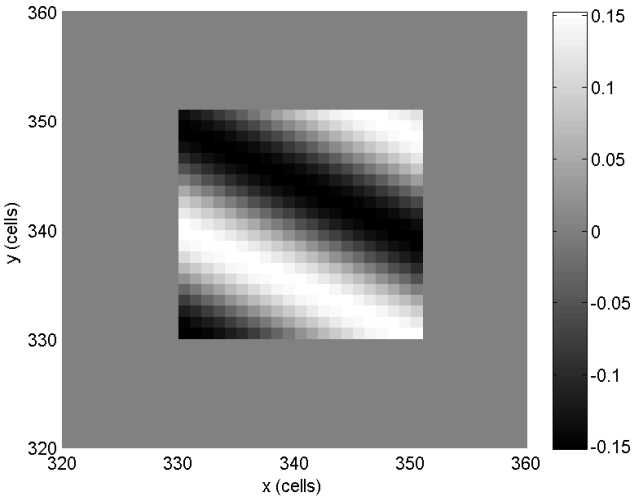

Fig. 3. E_z field in the 3-D TFSF FDTD domain with the plane wave propagating from lower-left to upper-right corner ($\phi = 63.4°$, $\theta = 36.7°$, $\psi = 26.6°$, $m_x = 1$, $m_y = 2$, $m_z = 3$) at time $n = 130$ steps.

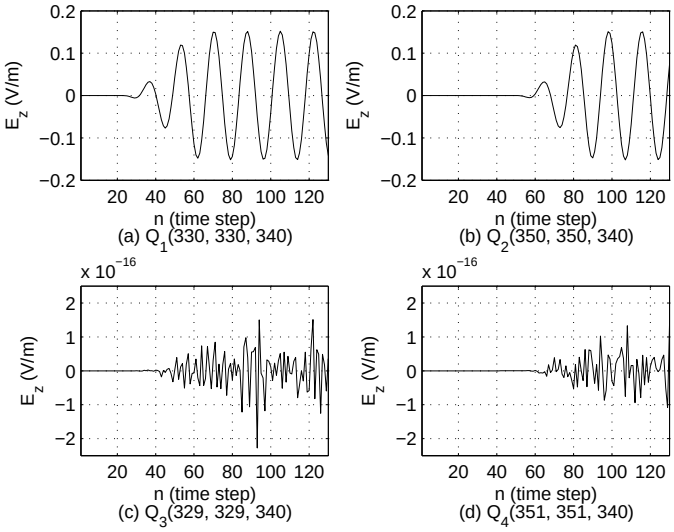

Fig. 4. Electric field measured in (a)–(b) total-field and (c)–(d) scattered-field regions of the TFSF FDTD domain. Simulation parameters are the same as for the results in Fig. 3.

thus the presented AFP implementation is validated.

In Fig. 4, E_z-field waveforms measured in the corners of the TFSF interface in the FDTD domain are presented. The positions of the measurement points Q_1–Q_4 are determined in the coordinate system shown in Fig. 3. As seen, the fields measured in the scattered-field region are almost 16 orders of magnitude lower than the amplitude of the plane wave in the total-field region.

The computational efficiency of DPW implemented with the use of (41)–(42) is much lower than the original DPW implementation based on the update of 6 auxiliary 1-D grids [7]. It stems from the requirement of MPA in computations of DGF. Therefore, the presented benchmarking simulations are executed for small total-field domains of size $21 \times 21 \times 21$ cells. However, the presented implementation of DPW does not require the termination of auxiliary 1-D grids by an absorbing boundary condition (cf. [7]). The convolution formulation of DPW obtained in the time domain is based on a kernel which is not an elementary function. Hence, the presented convolution formulation of DPW does not provide significant advantages in comparison with the DGF formulation in the frequency domain [2], [3], [4].

IV. Conclusion

The closed-form expression for the time-domain Green's function of DPW propagating in the 3-D FDTD grid is derived. It is verified that this expression allows to perfectly inject DPW at the TFSF interface. Due to the computational overhead, the derived DPW formulation has limited applicability in FDTD simulations. The developed methodology based on the multidimensional $\mathcal{Z}$–transform can be useful for derivations of integral DPW representations in other finite-difference schemes. The results obtained facilitate theoretical investigations in the area of the FDTD method.

References

[1] A. Taflove and S. C. Hagness, *Computational Electrodynamics: The Finite-Difference Time-Domain Method*, 3rd ed. Boston, MA: Artech House, 2005.

[2] C. D. Moss, F. L. Teixeira, and J. A. Kong, "Analysis and compensation of numerical dispersion in the FDTD method for layered, anisotropic media," *IEEE Trans. Antennas Propag.*, vol. 50, no. 9, pp. 1174–1184, Sep. 2002.

[3] J. B. Schneider "Plane waves in FDTD simulations and a nearly perfect total-field/scattered-field boundary," *IEEE Trans. Antennas Propag.*, vol. 52, no. 12, pp. 3280–3287, Dec. 2004.

[4] T. Tan and M. Potter, "Optimized analytic field propagator (O-AFP) for plane wave injection in FDTD simulations," *IEEE Trans. Antennas Propag.*, vol. 58, no. 3, pp. 824–831, March 2010.

[5] T. Tan and M. Potter, "1-D multipoint auxiliary source propagator for the total-field/scattered-field FDTD formulation," *IEEE Antennas Wireless Propag. Lett*, vol. 6, pp. 144–148, 2007.

[6] T. Tan and M. Potter, "On the nature of numerical plane waves in FDTD," *IEEE Antennas Wireless Propag. Lett*, vol. 8, pp. 505–508, 2009.

[7] T. Tan and M. Potter, "FDTD discrete planewave (FDTD-DPW) formulation for a perfectly matched source in TFSF simulations," *IEEE Trans. Antennas Propag.*, vol. 58, no. 8, pp. 2641–2648, Aug. 2010.

[8] J. Vazquez and C. G. Parini, "Discrete Green's function formulation of FDTD method for electromagnetic modelling," *Electron. Lett.*, vol. 35, no. 7, pp. 554–555, Apr. 1999.

[9] R. Holtzman and R. Kastner, The time-domain discrete Green's function method (GFM) characterizing the FDTD grid boundary," *IEEE Trans. Antennas Propag.*, vol. 49, no. 7, pp. 1079–1093, Jul. 2001.

[10] W. Ma, M. R. Rayner, and C. G. Parini, "Discrete Green's function formulation of the FDTD method and its application in antenna modeling," *IEEE Trans. Antennas Propag.*, vol. 53, no. 1, pp. 339–346, Jan. 2005.

[11] R. Kastner, "A multidimensional Z-transform evaluation of the discrete finite difference time domain Green's function," *IEEE Trans. Antennas Propag.*, vol. 54, no. 4, pp. 1215–1222, Apr. 2006.

[12] T. P. Stefanski, "A new expression for the 3-D dyadic FDTD-compatible Green's function based on multidimensional Z-transform," *IEEE Antennas Wireless Propag. Lett*, vol. 14, pp. 1002–1005, 2015.

[13] T. P. Stefanski, "Analytical expression for the time-domain discrete Green's function of a plane wave propagating in the 2-D FDTD grid," *IEEE Antennas Wireless Propag. Lett*, vol. 13, pp. 887–890, 2014.

[14] D. E. Dudgeon and R. M. Mersereau, *Multidimensional Digital Signal Processing*, Prentice-Hall Signal Processing Series Englewood Cliffs, N.J, USA: Prentice Hall, 1984.

[15] MATLAB Release 2010a, The MathWorks, Inc., Natick, Massachusetts, United States.

[16] T. P. Stefanski, "Electromagnetic problems requiring high-precision computations," *IEEE Antennas Propag. Mag.*, vol. 55, no. 2, pp. 344–353, April 2013.
[17] T. Granlund, "The multiple precision integers and rationals library (Edition 2.2.1)," GMP Development Team, 2010 [Online]. Available: http://www.mpir.org
[18] T. Nakayama and D. Takahashi, "Implementation of multiple-precision floating-point arithmetic library for GPU computing," in Proc. 23rd IASTED PDCS, Dec. 1416, 2011, pp. 343–349.

Tomasz Stefański received the M.Sc. degree in telecommunications and the Ph.D. degree in electronics engineering, from Gdansk University of Technology (GUT), Gdansk, Poland, in 2002 and 2007, respectively. He is currently an Assistant Professor at the Faculty of Electronics, Telecommunications and Informatics at GUT. Before joining GUT in 2011, he was with the Swiss Federal Institute of Technology (ETH Zurich) conducting research on parallelization of electromagnetic solvers on modern computing architectures using OpenCL programming language. Between 2006 and 2009 he worked at the University of Glasgow developing parallel alternating direction implicit finite-difference time-domain (ADI-FDTD) full-wave solvers for general purpose high-performance computers and graphics processing units. His current research interests include parallel processing and computational electromagnetics.

Bartosz Reichel was born in Gdansk, Poland. He received the M.Sc. degree in Applied Physics from the Gdansk University of Technology, Poland, in 2004 and the Ph.D. degree in Theoretical Physics from the same university in 2008. His previous works were related to computational electrodynamics connected with light propagation in nonlinear media and microwave propagation. His current research interest include plasmonic phenomena in metals and metamaterials.